Fundamental diagram of traffic flows on urban roads – local versus whole-link approaches

Peter Wagner (corresponding author)
Institute of Transportation Systems,
German Aerospace Centre, 12489 Berlin, Germany
phone: +49 30 67055-237, fax: +49 30 67055-291
email: peter.wagner@dlr.de, web: http://www.dlr.de/ts/

Elmar Brockfeld,
Institute of Transportation Systems,
German Aerospace Centre, 12489 Berlin, Germany
phone: +49 30 67055-231, fax: +49 30 67055-291
email: elmar.brockfeld@dlr.de, web: http://www.dlr.de/ts/

Nathan H. Gartner,
Dept. of Civil and Env'l engineering,
University of Massachusetts, Lowell, MA 01854, USA
phone: +1 978-934-2289, fax: +1 978-934-3052
email: Nathan_Gartner@uml.edu

Alexander Sohr
Institute of Transportation Systems,
German Aerospace Centre, 12489 Berlin, Germany
phone: +49 30 67055-458, fax: +49 30 67055-291
email: Alexander.sohr@dlr.de, web: http://www.dlr.de/ts/

Date: 8. March 2009

Word count: 4229 + 12 figures = 7229

Abstract

Fundamental diagrams of traffic flow variables have been quite useful in determining freeway operations quality. However, they are usually not used for that purpose on urban roads. This work is an approach towards utilizing the fundamental diagram on urban roads, too. Based on a host of empirical as well as simulation work, the first steps towards a routine application of the fundamental diagram are sketched. In addition, two approaches are compared, one that uses a traditional fundamental diagram as measured by loop detectors, and the second one which uses a whole-link approach relating link-travel-speed with volume. Especially the travel times contain important information that can be used for traffic management applications.

1 Introduction

It is well-known, that the form of the fundamental diagram (1) depends on the location where it is measured (2). This is true on freeways, and it is especially true for urban roads (see Fig. 2 as an example). There are three locations to be discerned: before and after the signal or the intersection, where a large share of vehicles is either accelerating or decelerating, and hence traffic flow is strongly non-stationary, and in between two signals, where traffic flow is more homogeneous.

In previous work (3), a simplified approach has been used which was a simulation on a closed ring together with a number of traffic signals. Since the global density k on the ring is in this case the control variable, the fundamental diagram can be displayed as a three-dimensional function of the traffic flow $q(k,\phi)$ versus density k and offset ϕ.

When discussing the open urban road (4), (5), (6), (7), (8), such as the simple example in Fig. 2 which will be used in the following, the density is no longer the control variable. Instead, such a system is controlled by the flow that goes into it (q_{in}) and the flow that can leave it (q_{out}). These numbers, together of course with the traffic signal settings will determine the density k and the overall performance of the section under consideration.

2 The simulation set-up

The simulations have been performed with a simple three-link network depicted in Fig. 1. The microscopic simulation model used is a stochastic variant (9) of the well-known Gipps model (10):

$$v(t+h) = \min\{v(t) + ah, v_{\max}, v_{safe}\} - \sigma_a \xi. \quad (1)$$

$$v_{safe} = -b\tau + \sqrt{b^2\tau^2 + V^2(t) + 2bg(t)}. \quad (2)$$

$$x(t+h)=x(t)+hv(t+h). \quad (3)$$

Here, $x(t)$,$v(t)$ is the vehicle's position and speed at time t, $g(t)=X(t)-x(t)-\ell$ is the spatial headway to the lead vehicle whose speed is $V(t)$ and position $X(t)$. The parameter ℓ is the vehicle length; h is the time-step size which has been set to 1 s for all the simulation runs in the following. The variable $\xi(t)$ is a random number drawn from the interval [0,1]. The parameters are a (maximum acceleration), b (maximum deceleration), v_{max} (maximum speed), τ (preferred time headway), and the acceleration noise σ_a.

Only data from the link in the middle have been collected, to minimize the effect of the somewhat unnatural boundary conditions. The upstream boundary is fed with vehicles drawn from a Poisson distribution which enter the network with the maximum safe speed possible and lead to the desired inflow q_{in}. Note that for large values of the inflow q_{in} not all vehicles can enter the network, since this would violate the safety condition of the car-following model. Therefore, inflow is effectively limited to a certain value which is given by the total capacity of the system. Of course, temporarily larger inflows are possible.

The downstream boundary is simply left open, i.e. any vehicle that reaches the downstream end is removed from the system. Another possibility would have been to prescribe explicit

boundary conditions here (by specifying either q_{out} or v_{out}), the vehicles must then be forced to follow these boundary conditions. However, this would have added another line of complexity, which is currently not needed. It is simpler to handle the outflow condition by the traffic light on the last link: by making its green times shorter than the ones of the upstream signals, a downstream bottleneck can be created.

Since this article is mainly interested in congested conditions, the traffic signals in the simulation are not very well co-ordinated. They run at a fixed cycle control with cycle time C=90 s and different green times G=45…60 s. To increase the level of congestion and make it comparable with the empirical data in section 3, the downstream signal is sometimes run at a shorter green time than the two upstream signals.

From this simulation set-up, the data have been recorded from the three loop detectors. In the simulation, a vehicle that crosses the position of a loop simply records its speed – no efforts had been made to model explicitly a double loop detector and how it derives the variables from the measurements. This virtual loop records single vehicle data which can be aggregated into averages or into frequency distributions.

Note, that only speeds v_i and flows q (more precisely: the moments in time t_i when a vehicle crosses the loop detector) have been used, since double loop detectors cannot report the density. For the fundamental diagrams, the simulations were run with a fixed inflow for several simulated hours. This was repeated for different levels of inflow, which creates different levels of saturation in the simulation area. All these measurements were collated into the fundamental diagrams in Fig. 2. In addition, the parameters of the vehicle dynamics, especially the maximum speed, are distributed among the vehicles in a certain range ±2 m/s around the admissible speed in Germany's cities, which is 50 km/h (13.88 m/s).

It can be seen, that the maximum reachable flow depends only weakly on the length of the time interval, different from highway fundamental diagrams. For aggregation times larger than the cycle time, the maximum flow does not show any dependence on aggregation, especially if the aggregation time is a multiple of the cycle time. Furthermore, especially close to the signal, the fundamental diagram takes a form that has not been reported (to our knowledge) in the literature before. This is due to the fact, that basically two vehicle populations are averaged over in this plot: the vehicles that are almost standing, and the ones which can drive (during the green period) with normal speed. The details will be given in the next paragraph, with the help of an analysis of the speed distributions.

2.1 Interpretation

The interpretation of these simulation results can be given when analyzing the frequency distributions of the speeds. The simplest to understand is of course the loop in the middle – it usually is far away from the disturbances caused by the signals. In Fig. 3 this is demonstrated (grey line, right plot of Fig. 3): for normal conditions, the speeds are approximately normally distributed around the expected speed limit.

The black curve in Fig. 3 (right) is closer to the upstream traffic signal, so vehicles have not yet reached the allowed speed but are driving slower – therefore, the black line's peak value is a bit below the grey line's peak value.

Finally, when going even closer to the signal, the speed distribution becomes bi-modal (left plot of Fig. 3): just 30 m downstream of a traffic signal, vehicles may belong to one out of two

populations: the vehicles which had crossed the intersection almost undiminished in speed, and the ones who had come to a complete stop and must now accelerate again. At this point, they have just reached the speed of 7 m/s, which fits well to their average acceleration of 1 m/s^2 (which is one of the parameters of the model).

The situation is more complicated immediately upstream of the traffic light, see Fig. 4. Here, the distribution changes from small volume (black solid curve) to medium (grey solid curve) and to large volume (dotted curve). For small volumes, most vehicles can go almost at full speed. That they do not reach full speed is due to the bad co-ordination between this signal and the upstream signal, vehicles have to decelerate before the signal switches to green. For increasing volumes this effect becomes stronger, leading to a decrease in the peak speed. In addition, the population of completely stopped vehicles grows, and with it the peak at small speeds. At still larger volumes, even the downstream congestion influences the speed distributions, with peak speed going down even more.

From this analysis, it is understood why the fundamental diagram especially in the vicinity of the traffic light looks unusual. And it should have become evident by the discussion above, that the fundamental diagram contains information about the signal settings itself, and even about the co-ordination between this signal and the signal upstream – provided, it is not too far away as is the case in the empirical data that are to reported next.

3 The empirical set-up

To support and extend the simulation results, data from DLR's urban road research laboratory were also used. Fig. 5 shows a sketch of the area. Only the data of the eastbound traffic were used in the following, since there is a strong bottleneck downstream that causes congestion to travel backwards until it encroaches the area under surveillance. This is due to a strong demand especially in the late afternoon, where a lot of commuters return home, and some ongoing construction work which had reduced the capacity of the surrounding net.

The Fig. 6 is constructed similar to the simulation results in Fig. 2, with some slight differences.

In any case, the original data to be used have been single vehicle data which where then aggregated into the fundamental diagrams in Fig. 6. Different from the simulation set-up, the next upstream traffic light is almost 1.5 km apart from of the signal we are analyzing. So, the influence caused by this light has almost vanished and it needs not be discussed. The signal parameters are unfortunately not known, the signals are run with a traffic actuated control scheme, which however is not adapted to the congestion in the late afternoon. When comparing Fig. 6 to the simulation results in Fig. 2 it could be seen, that the empirical data display more noise than the simulation data. Also, especially the fundamental diagram upstream of the signal looks different from the one in the simulation. The other two fundamental diagrams nevertheless compare well to their simulation counterpart.

The empirical speed distributions are a certainly easier to interpret than the fundamental diagrams. In Fig. 7 it could be seen how the speed distribution changes with the distance to the signal. While at the detector in between only standing or driving vehicles are observed, the other two detector sites around the signal display a surprisingly small share of standing vehicles; the host of vehicles are still moving, albeit with smaller speeds.

The corresponding fundamental diagrams in Fig. 8 demonstrate that there is a difference between a fundamental diagram at an intersection when the congestion is generated downstream versus a signal without such a congestion downstream. Albeit these preliminary results need a more in-depth investigation, it demonstrates the lines along which such fundamental diagrams can be used to do performance numbers of intersections.

4 The travel times / link performance function

Having described so far what happens locally, at the level of the individual loop detectors, more information can be gained by switching to the representation of a whole link. In this case it is more appropriate to use the travel-speed V versus demand q representation $V(q)$, since it encapsulates the performance of a link into a simple function which is so similar to a fundamental diagram that it still deserves the name.

4.1 Comparing local speeds with link speeds

Albeit the whole-link fundamental diagram looks similar to its local counterpart (see Fig. 11 for the simulation results, and Fig. 12 for empirical examples), the variables to be plotted against each other are definitely different from the local fundamental diagram above. This is especially true for the speed and it is demonstrated in the following Fig. 9 for the simulation as well as for a set of empirical data. In Fig. 9, the difference between local speed and travel speed is shown, both for the simulated as well as for the empirical data. This has been done in the form of a frequency distribution in the v,V–plane, in order to help recognizing characteristic features of the two data-sets. Simulation data and empirical data share the feature of displaying a large cloud of data around v=50 km/h; the simulation data in addition display a branch that connects this data-cloud with the origin. These data are from a completely congested situation, which was prepared for the simulation data but was not present in the empirical data. In any case it is clear, that the travel speed is not a simple linear function of the local speed. Both variables carry different information.

This outcome is due to the fact, that the loop detector between two intersections rarely experience congestion, which would cause its speed to go down, too. The travel speed, however, is sensitive to the congestion caused by the downstream intersection (and any other congestion as well, of course) and therefore reacts to the level of congestion. Oversimplifying what is happening here, one gets for one local speed a wide range of travel speeds, and this is what is being displayed in Fig. 9. Of course, if congestion becomes larger, then finally even the local speed will go down, and with it the travel speed.

This means, that the travel times (travel speeds) are very well suited for traffic management applications. The local speeds are not so simple to utilize in this respect, their usefulness depends on the location of the detector. By putting the loop detector in between two traffic signals, its speed information is not as worthy (however, the volume still is) as the travel speeds.

4.2 Link performance functions

For the case of a single intersection, there is already a very good theoretical description available, although it is usually not regarded as such: the delay time d, and with it the travel time $\Phi(\cdot)$ can

be quite accurately described by Webster's equation (11), which relates demand q_{in} to travel time, and, along with this, to travel speed.

$$d(q=q_{in}) = \frac{C}{2}\frac{\left(1-\frac{G}{C}\right)^2}{1-\frac{C}{G}\frac{q}{Q}} + \frac{\left(\frac{q}{Q}\right)^2}{2q\left(1-\frac{q}{Q}\right)} - 0.65\left(\frac{C}{q^2}\right)^{\frac{1}{3}}\left(\frac{q}{Q}\right)^{2+5\frac{G}{C}} \qquad (4)$$

where Q is the maximum flow (throughput), G is the effective green time, and C is the cycle time of the signal.

In this case, a link fundamental diagram can be defined quite clearly, however, it is only the mean value which is simple: the distribution of delays $p(d)$ does not follow a simple normal distribution. This is due to the fact, that this distribution is bi-modal: a vehicle has a certain chance to pass the intersection without stopping (peak around small delays) or it can be stopped by the intersection, incurring a large delay.

The aforementioned fundamental diagram can be now defined by noting that the travel time and the travel speed V are related to e.g. Webster's delay approximately (where v_{free} is the speed limit on that link, and L is the length of the link):

$$V(q) = \frac{L}{L/v_{free} + d(q)} \qquad (5)$$

which is depicted in Fig. 10. It is important to note that although the curve $V(q)$ extends to $V=0$ (for $q = \frac{G}{C}Q$ it becomes zero, because here the signal reaches capacity), in the real simulation no travel speeds smaller than a minimum speed will be observed, provided the downstream link is always free. This is due to the fact that the maximum travel time (on a link with finite length and with outflow capacity $\frac{G}{C}Q$ is just given by

$$\Phi_{\max} = \frac{n}{\frac{G}{C}Q}$$

where n is the maximum number of vehicles that fit on the link. Therefore, travel speeds smaller than

$$V_{\min} = \frac{L}{\Phi_{\max}} = \langle \ell \rangle \frac{G}{C} Q$$

can only occur if there is downstream congestion or if an incident is present at the current link. (Here, $\langle \ell \rangle$ is the average vehicle length.) The downstream congestion has the effect of decreasing the (effective) green time G. Alternatively, it is possible to model this situation also by a reduction of Q, however Q is more likely to be affected by weather conditions and not by the downstream congestion. So the congested branch in the measured link performance functions is related to downstream congestion, it is not possible to produce it internally.

Interestingly, at least the uncongested branch of the fundamental diagram can be described by Eq. (4), see Fig. 11 for an example.

So far, simulation results have been used to describe the most important features of the link performance function. They will be compared in the following with empirical data. The data used for this purpose have been sampled in 2007 in the VLS-area in Nuremberg, Germany, where both loop detection as well as floating car data had been available. The data have been recorded for four months, and along with the travel times, the traffic flows have been measured. Both

variables have been aggregated into 20 minutes bins, Fig. 12 shows the resulting frequency distributions for four different locations.

5 Conclusions

This work has discussed two possible approaches to do performance measurements in urban roads: one that is based on traditional data like loop detector data, and a second one that is based on travel times and travel speeds, together with a measurement of traffic flow. These data can be expected to be available in the near future with the further progress of vehicle infrastructure integration (VII).

It has been demonstrated, that even a fundamental diagram taken directly in front of a traffic signal contains valuable information. This information can be used to estimate the quality of the operation of the intersection; additionally, the fundamental diagram contains information about the quality of the progression between two intersections. However, it is not completely straightforward to relate the fundamental diagram to a level of service. One approach might be the one discussed in (4) to analyse the loop data together with the information from the traffic signal about its current state. E.g., if the congestion is generated downstream, then the vehicles have a big chance not to move despite the fact that the signal is green. So, if the congestion is caused at the signal itself, one should find an almost undiminished outflow which can be observed very well either by a detector either upstream or downstream, but close to the signal. More work is clearly needed to turn these observations into a working method for a better quality management.

However, we think that even more information can be obtained from travel-time (or travel speed) versus demand functions (link performance functions). As has been demonstrated in section 4, the travel time data contain valuable information about the loss times experienced by the vehicles, and this information can be used directly as input information for traffic management. Although these data are still not commonly in use, they will become much more frequently available soon, e.g. with the further progress of VII or with other technologies that can follow the trajectory of a vehicle for a certain distance to determine travel times or delay times (e.g. video).

Finally, it has been demonstrated that at least the link performance function can be described analytically to a certain degree. In this article, it has been done with the help of Webster's delay formula, however by using other approaches even more useful description might be derived. This would help in assigning levels of service to a given situation, which will open the road to a better performance and quality management.

References

(1) Greenshields, B.D., A Study in Highway Capacity. *Highway Research Board*, Proceedings, Vol. 14, 1935, p. 458.

(2) Hall, F.L., V.F. Hurdle, and J.M Banks, Synthesis of recent work on the nature of speed-flow and flow-occupancy (or density) relationships on freeways, *Transportation Research Record: Journal of the Transportation Research Board* 1365, 12 – 17 (1992).

(3) Gartner, N.H. and P. Wagner, Traffic flow characteristics on signalized arterials, *Transportation Research Record: Journal of the Transportation Research Board* No. 1883, 2005, pp 94 – 100.
(4) Henry X. Liu, Xinkai Wu, and Nikolas Geroliminis, Fundamental Diagram for Signalized Arterials: An Empirical Analysis using High-Resolution Traffic Data, presented at the Woods Hole meeting Greenshields Symposium (2008).
(5) Hallenbeck, Mark E, Ishimaru, John M, Davis, Katherine D, Kang, Jaime M, Arterial Performance Monitoring Using Stop Bar Sensor Data, presented at *Transportation Research Board* 87th Annual Meeting (2008).
(6) Nee, J. and M. E. Hallenbeck, Surveillance Options for Monitoring Arterial Traffic Conditions, Technical Report, Washington State Transportation Center (2001).
(7) Huang D.-W. and W.-H. Huang. Traffic signal synchronization, *Physical Review E* 67, 2003, 056124
(8) Daganzo, C.F. and N. Geroliminis, An analytical approximation for the macroscopic fundamental diagram of urban traffic, *Transportation Research B* 42, 2008, pp 771 – 781.
(9) Krauß, S, P. Wagner, and C. Gawron, Metastable states in a microscopic model of traffic flow, *Physical Review E* 55, 1997, pp 5597 – 5605.
(10) Gipps, P.G., A behavioural car following model for computer simulation, *Transportation Research B* 15, 1981, pp. 105–111.
(11) Webster, F. V., *Traffic Signal Settings*, Her Majesty's Stationery Office, Road Research Technical Paper No. 39, Department of Scientific And Industrial Research Road Research Laboratory, 1958.

Figure Captions

Figure 1: Road scenario used for microscopic simulations. The loop detectors are located at three locations, downstream of the first signal (x=30 m), between two signals (x=300 m), and upstream of the second signal (x=570 m).

Figure 2: Fundamental diagram at the three different locations shown in Fig. 1 (x=30, 300, 570 m) and for three different aggregation intervals T=60, 180, 300 s. Demand was changed stepwise from 36 veh/h to 1260 veh/h in steps of 36 veh/h, where each level of inflow had been held constant for about five simulated hours.

Figure 3: Frequency distribution of the simulated speeds, measured at the three different locations (left, x=30 m, right, x=100, 300 m).

Figure 4: Frequency distribution of the simulated speeds, measured at the location directly upstream of the traffic light. The curves are for different inflows (q=0.05, 0.1, 0.2 veh/s), the different height of the curves is due to the fact that the distributions are un-normalized. The green times of the three signals were 45 s, so delays are only due to bad co-ordination.

Figure 5: Sketch of DLR's urban road research laboratory, where the measurements displayed in Fig. 6 have been performed. It is a four-lane road (two lanes / direction). Note, that the loop detectors located at MQ 22 refers to the detector named "in between" in the simulation set-up, the detectors at MQ 41 refer to the upstream location and the detectors at MQ 42 to the downstream location.

Figure 6: Fundamental diagram obtained at the three different locations shown in Fig. 5 (downstream, in between, and upstream of the signal's position), and for three different aggregation intervals T=60, 180, 300 s. Note, these are now empirical data instead of simulated data. Data are from one week, between 16. May 2008 and 23. May 2008. In total, some 80,000 records have been used for the results reported here.

Figure 7: Empirical speed distributions for the three different locations shown in Fig. 5 (downstream, in between, and upstream of the signal's position). The plot is a cut through the fundamental diagram Fig. 6 at a flow value of 900 veh/h.

Figure 8: Fundamental diagram upstream and downstream of the signal. The left plot is for congested conditions, the right plot for uncongested conditions. (The uncongested data are from the opposite direction at the same intersection, where no bottleneck is located downstream.)

Figure 9: Comparison between the speeds measured at a loop detector between two intersections and the travel speed based on the measurement of travel time. Left plot shows the simulation data, the right plot is for the empirical data. The empirical data had been aggregated into 20 minutes bins and had been collected over four months to yield statistically meaningful results – the probe vehicle data density was very small.

Figure 10: Travel speed versus demand for a fixed cycle signal and for various green times. The parameters chosen are C=90 s and Q=0.5 veh/s.

Figure 11: Simulation results for the plot of the travel speed V versus the demand q, together with a fit to eq. (5). Fitting was done with a non-linear least-squares method that is implemented in the gnuplot software. The simulation parameters (inflow, sampling time) are the same as in Fig. 2.

Figure 12: Travel speed versus traffic flow for several real sites in Nuremberg. Similar patterns as the ones that had been observed in the simulation are visible, however so far nothing has been done to make this visual similarity more rigorous. The data are compiled from several months of raw data.

Figure 1

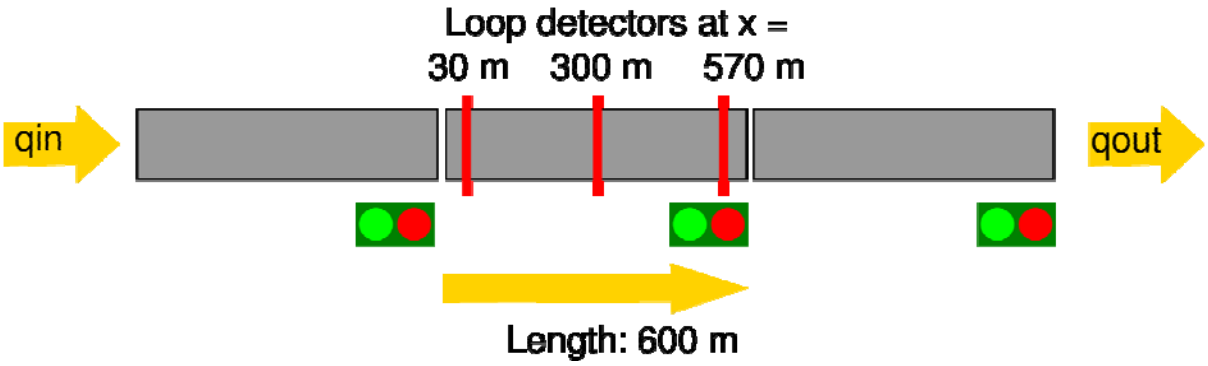

Figure 2

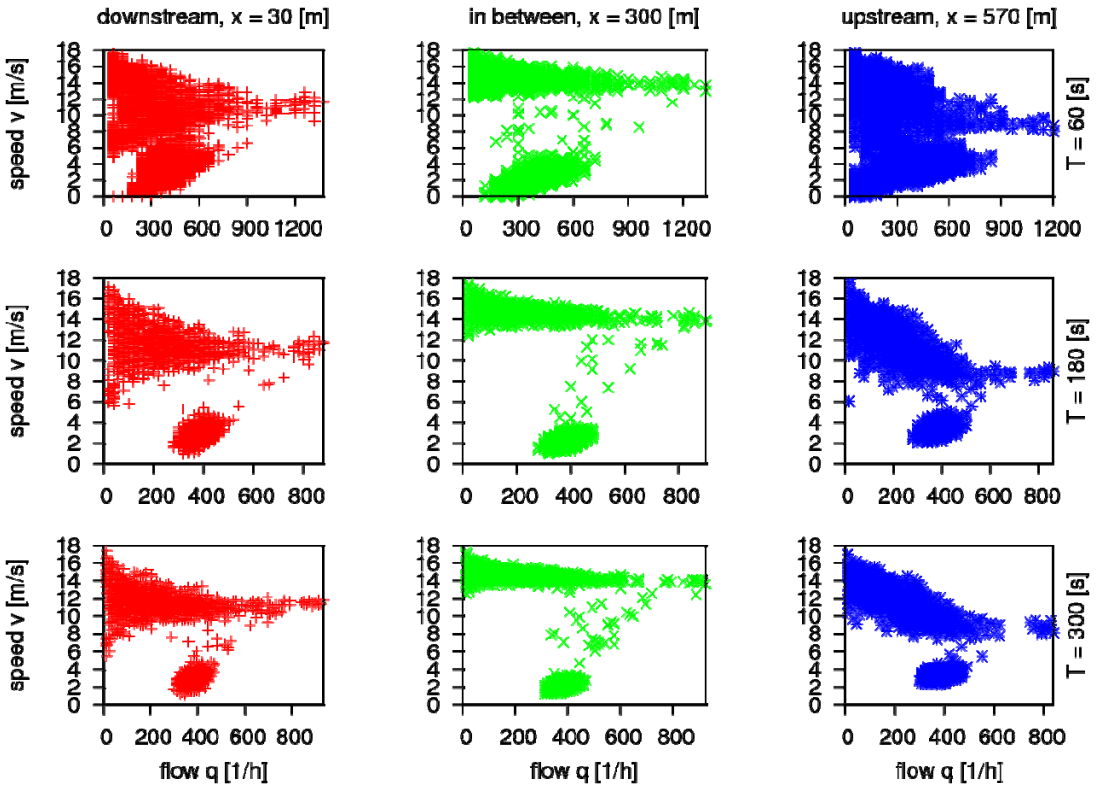
downstream, x = 30 [m]
in between, x = 300 [m]
upstream, x = 570 [m]
speed v [m/s]
flow q [1/h]
T = 60 [s]
T = 180 [s]
T = 300 [s]

Figure 3

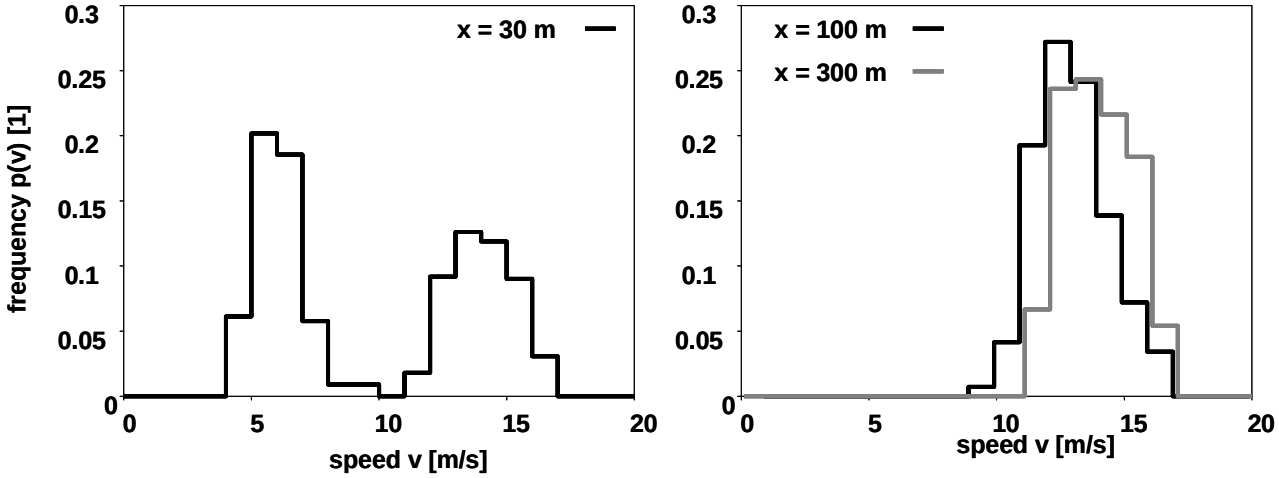

Figure 4

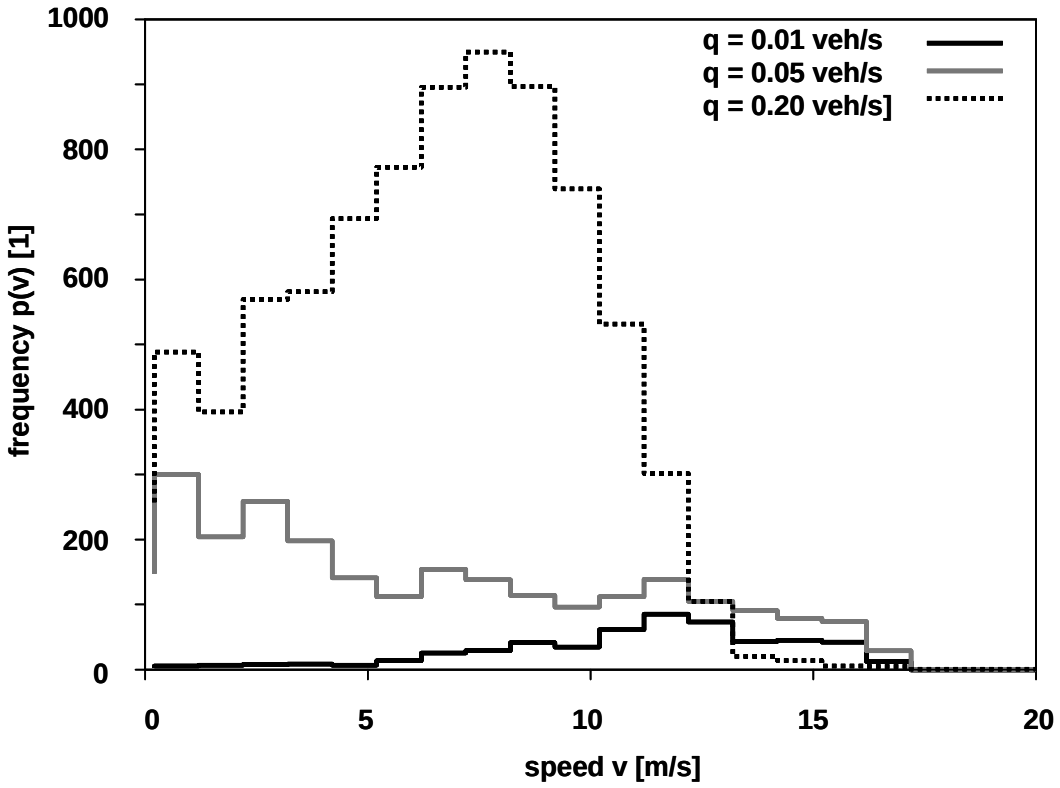
1000
800
600
400
200
0
frequency p(v) [1]
0
5
10
15
20
speed v [m/s]
q = 0.01 veh/s
q = 0.05 veh/s
q = 0.20 veh/s]

Figure 5

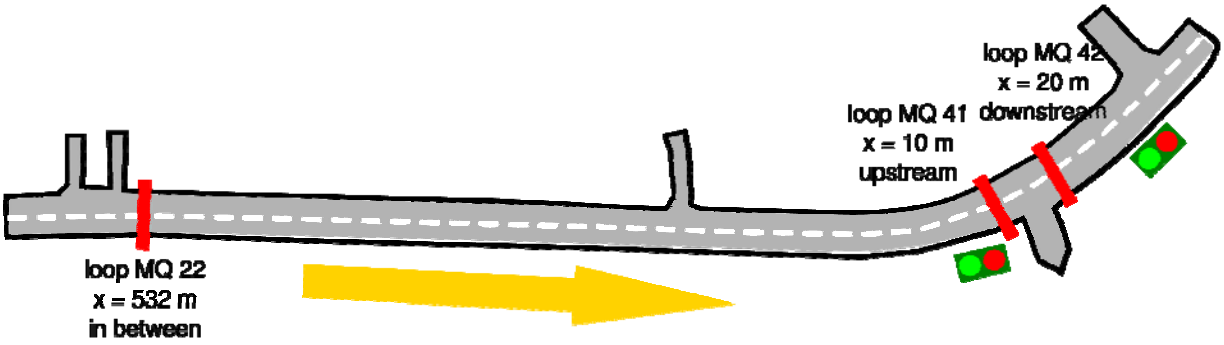
loop MQ 42
x = 20 m
downstream
loop MQ 41
x = 10 m
upstream
loop MQ 22
x = 532 m
in between

Figure 6

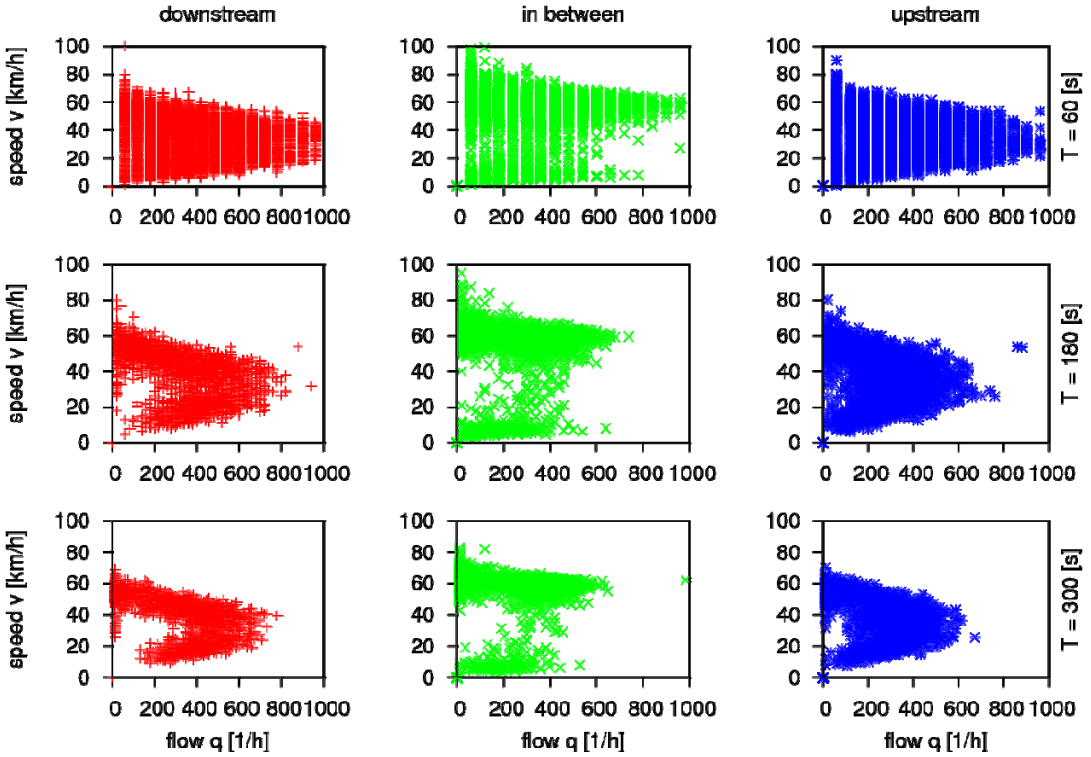
downstream
in between
upstream
speed v [km/h]
flow q [1/h]
T = 60 [s]
T = 180 [s]
T = 300 [s]
0
20
40
60
80
100
0 200 400 600 800 1000

Figure 7

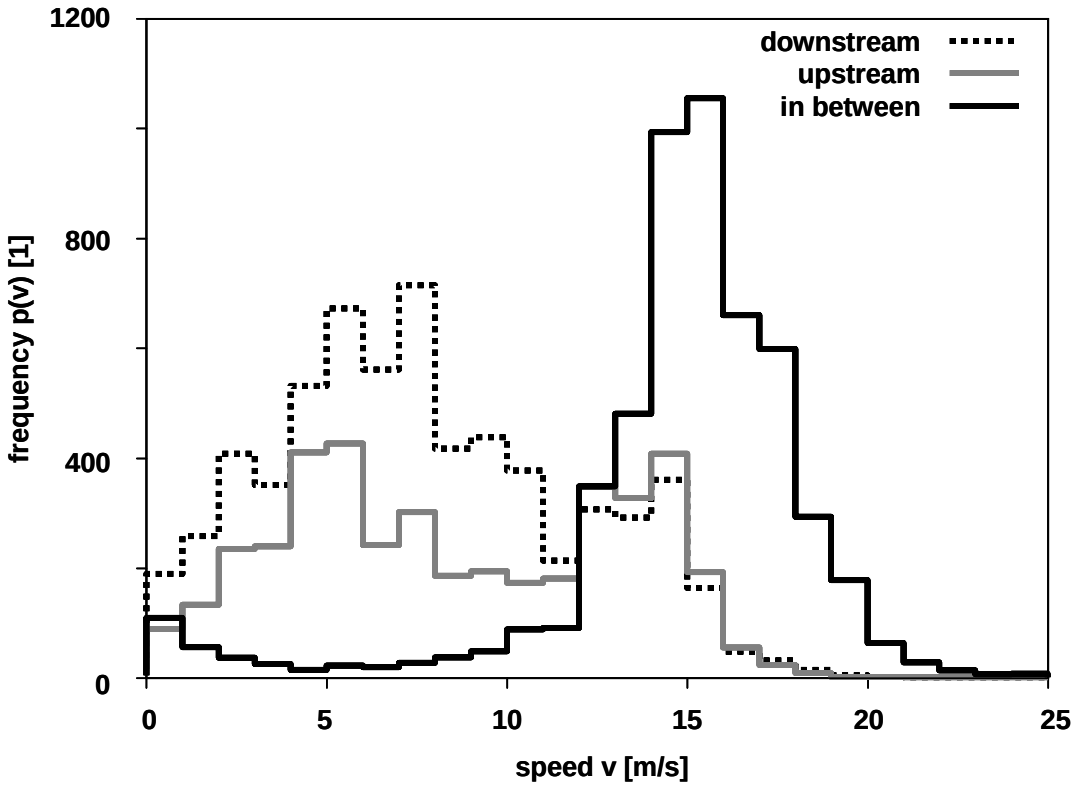
1200
800
400
0
frequency p(v) [1]
0
5
10
15
20
25
speed v [m/s]
downstream
upstream
in between

Figure 8

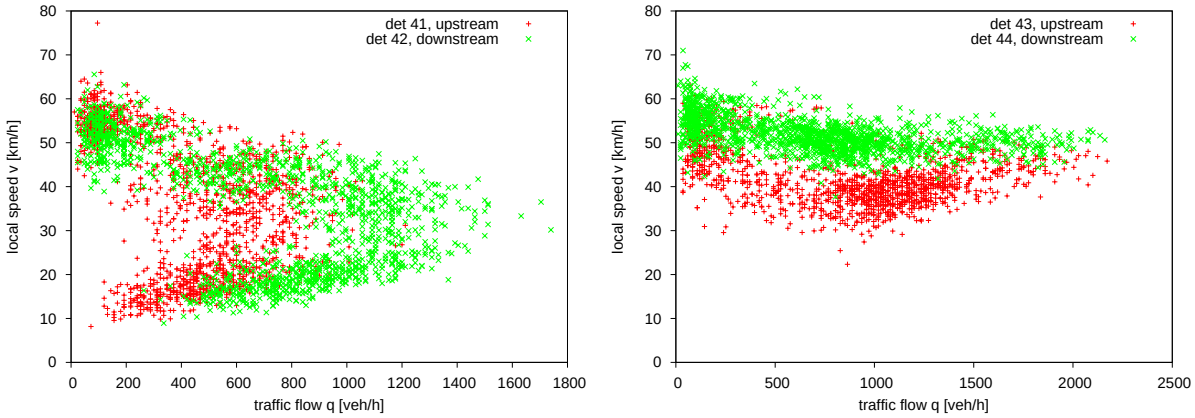
det 41, upstream
det 42, downstream
local speed v [km/h]
traffic flow q [veh/h]
0
10
20
30
40
50
60
70
80
0
200
400
600
800
1000
1200
1400
1600
1800
det 43, upstream
det 44, downstream
local speed v [km/h]
traffic flow q [veh/h]
0
500
1000
1500
2000
2500

Figure 9

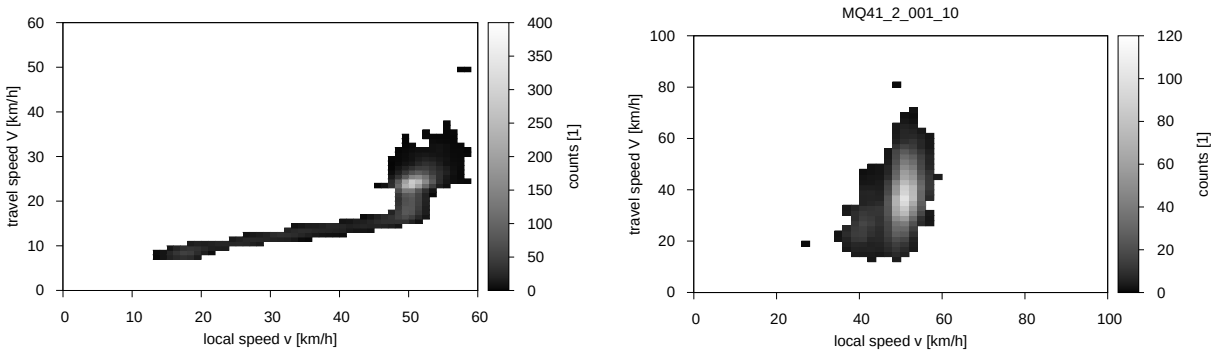

Figure 10

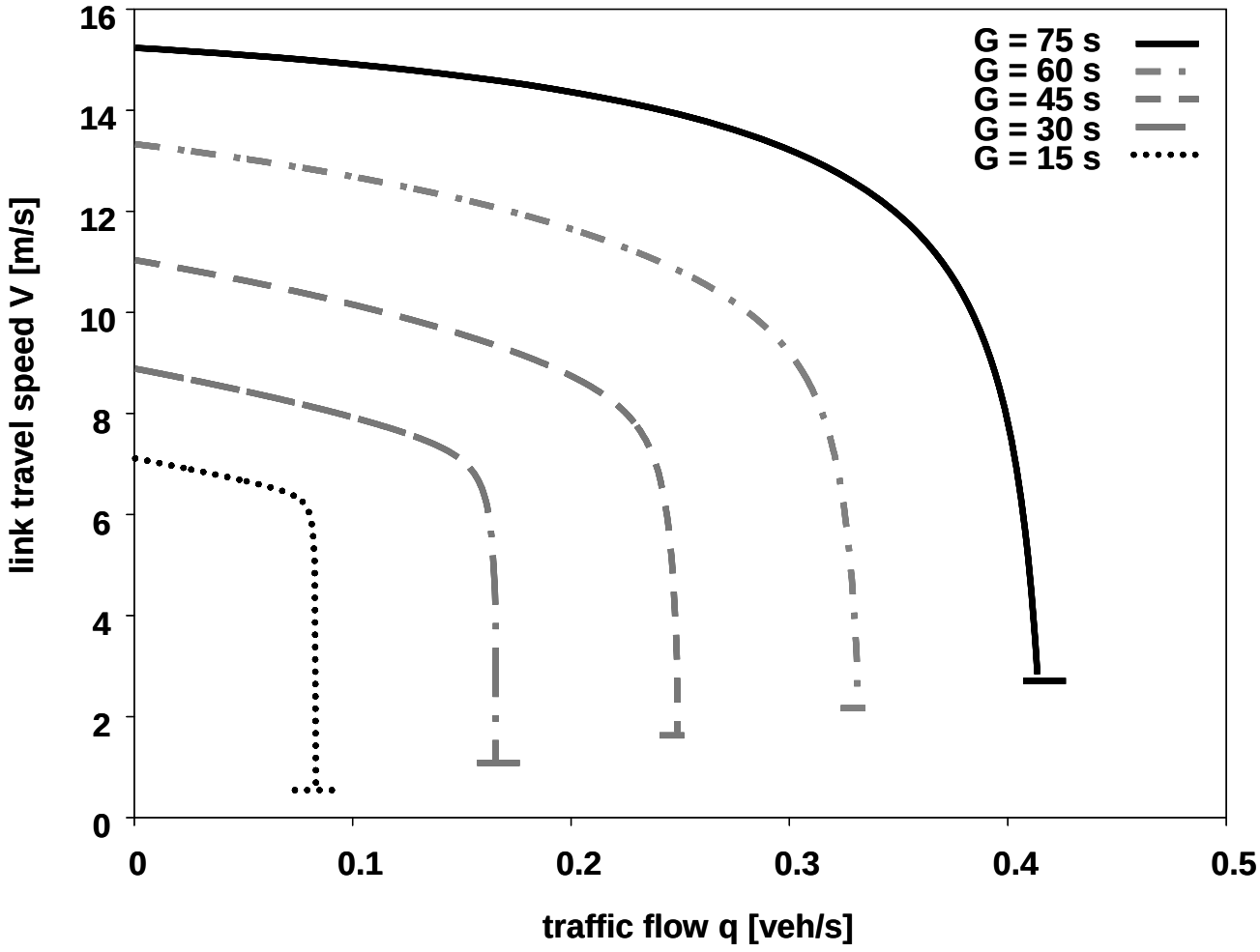
G = 75 s
G = 60 s
G = 45 s
G = 30 s
G = 15 s
link travel speed V [m/s]
traffic flow q [veh/s]
0
2
4
6
8
10
12
14
16
0
0.1
0.2
0.3
0.4
0.5

Figure 11

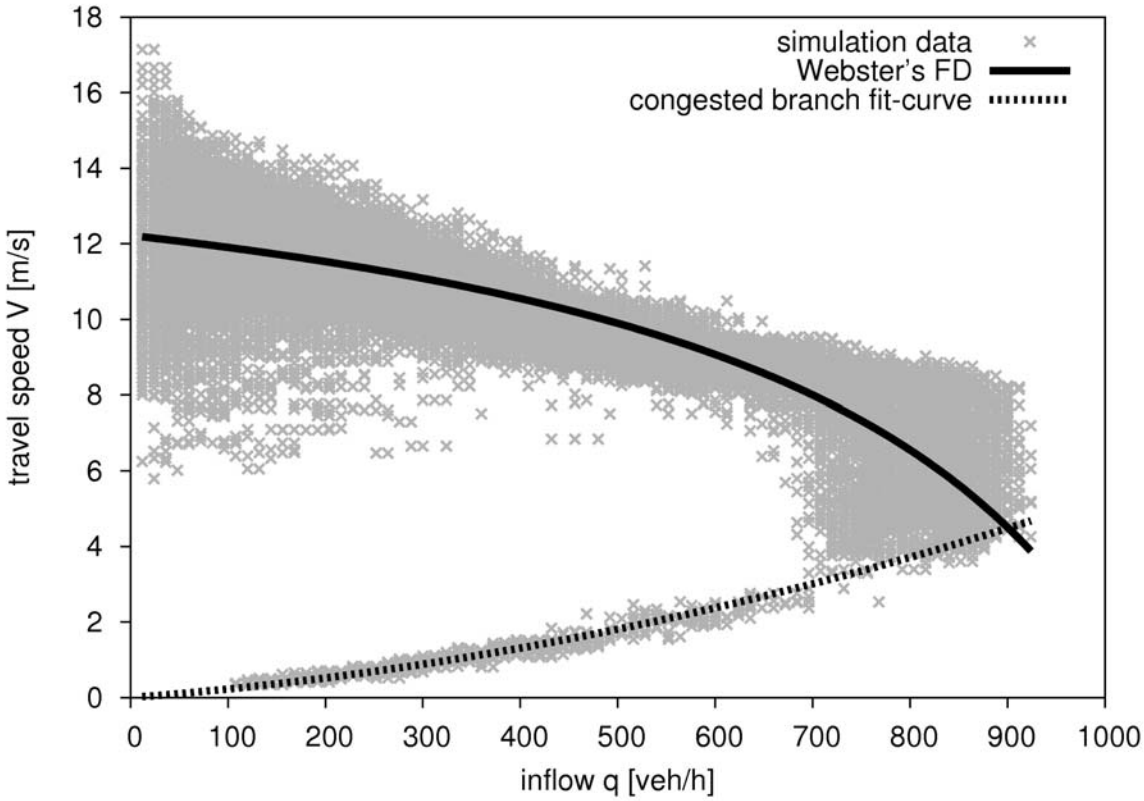
simulation data
Webster's FD
congested branch fit-curve
travel speed V [m/s]
inflow q [veh/h]
0
2
4
6
8
10
12
14
16
18
0
100
200
300
400
500
600
700
800
900
1000

Figure 12

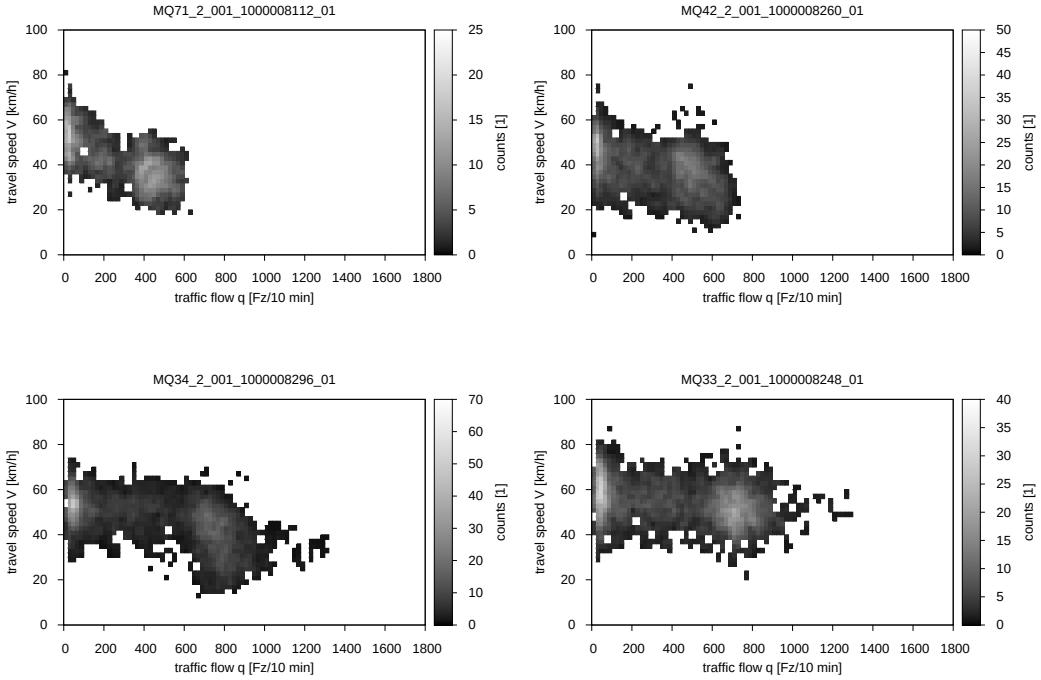
MQ71_2_001_1000008112_01
MQ42_2_001_1000008260_01
MQ34_2_001_1000008296_01
MQ33_2_001_1000008248_01
travel speed V [km/h]
traffic flow q [Fz/10 min]
counts [1]